THE ASTROPHYSICAL JOURNAL, 459:L69–L71, 1996 March 10

HIGH-VELOCITY MOLECULAR GAS IN THE GALACTIC CENTER RADIO LOBE

YOSHIAKI SOFUE
Institute of Astronomy, University of Tokyo, Mitaka, Tokyo 181, Japan; sofue@mtk.ioa.s.u-tokyo.ac.jp
Received 1995 August 11; accepted 1995 November 22

ABSTRACT

We point out a possible association of high-velocity molecular gas with the Galactic center radio lobe (GCL). A molecular spur in the eastern GCL ridge is receding at $V_{\rm LSR} \sim +100$ km s^{-1}, and the western spur approaching at $V_{\rm LSR} \sim -150$ km s^{-1}, suggesting a high-velocity rotation of the GCL. We study the kinematics of the GCL based on these molecular line data.

Subject headings: Galaxy: center — Galaxy: kinematics and dynamics — ISM: jets and outflows — ISM: molecules

1. INTRODUCTION

The Galactic center radio lobe (GCL) is the most prominent vertical object among various ejection structures in the nuclear region of the Milky Way, extending more than 200 pc in an Ω shape (Fig. 1, Pl. L10) (Sofue & Handa 1984; Sofue 1985). The lobe ridges comprise strong vertical magnetic fields of the order of a milligauss (Yusef-Zadeh, Morris, & Chance 1984; Tsuboi et al. 1986; Sofue et al. 1987). Although its outstanding appearance suggests a high-speed ejection, no kinematics has been obtained because of the lack of spectroscopic information. Recently, we (Sofue 1995a, b) studied three-dimensional structures of the nuclear ring and expanding features based on the ^{13}CO ($J = 1$–0) line data from the Bell Laboratories (BTL) survey (Bally et al. 1987). In the course of data analyses, we found high-velocity molecular features clearly associated with the GCL. In this Letter, we report the discovery of these peculiar features and investigate the kinematics of GCL for the first time.

2. RADIO CONTINUUM AND MOLECULAR LINE DISTRIBUTIONS

A radio continuum map of the Galactic center at 10.5 GHz observed with the Nobeyama 45 m radio telescope at a resolution of 2.′6 is shown in Figure 1 (*lower panel*) (Sofue 1985). The GCL comprises the prominent two-horned spurs at $l \sim 12'$ and $l \sim -35'$, extending toward positive latitudes. The eastern (*left-hand side*) ridge is an extension from the radio arc at $l = 12'$, and its negative-latitude extension is also clearly visible.

Molecular gas distributions are shown in Figure 2 (Plate L11). The top panel shows the integrated intensity map of the ^{13}CO ($J = 1$–0) line emission from the BTL survey. A molecular spur at $l \sim -30'$ is found in positional coincidence with the western (*right-hand side*) GCL ridge, extending toward positive latitudes, and its negative-latitude counterpart is also visible. However, no negative-b counterpart is present for the $l = 10'$ feature. Another enhanced ^{13}CO emission is found at $l \sim 10'$, $b \sim 10'$ associated with the eastern GCL ridge. As is shown later, these eastern and western molecular spurs comprise high-velocity gas at $V_{\rm LSR} \sim +100$ and -150 km s^{-1}, respectively. In order to see how the high-velocity gas is distributed, we obtained ^{13}CO intensities integrated from $V_{\rm LSR} = -160$ to -150 km s^{-1} for the western half and from $V_{\rm LSR} = +90$ to $+100$ km s^{-1} for the eastern half. The result is shown in a composite map in Figure 2 (*bottom*), where the ^{13}CO spurs now more clearly show up, resembling the two-horned continuum ridges. The eastern ^{13}CO clump is apparently connected to a broader feature extending toward $l \sim 20'$, $b \sim 15'$. However, this extended feature has an order of magnitude lower intensity and can be identified with the high-latitude part of the so-called 180 pc expanding ring at 150–180 km s^{-1} (Sofue 1995a). Moreover, the GCL clump has a sharp boundary at $l = 10'$. Therefore, the extended feature is more likely to be distinguishable from the GCL molecular clump. The GCL molecular clumps are also recognized in the total intensity distribution of the CS line emission from the BTL survey, which indicates that the GCL ridges contain high-density molecular gas.

Cross sections of the 10 GHz radio continuum and the molecular line intensities across the GCL ridges at $b = 10'$ are compared in Figure 3. Since the 10 GHz emission at $b = 10'$ is strongly contaminated by the radio halo of Sgr A, the GCL ridges do not clearly show up. So we also present a 10 GHz cross section at $b = 15'$, where the lobe ridges show up most clearly. The ^{13}CO and CS cross sections are almost identical to each other, and both are well correlated with the radio ridges. However, the molecular peaks are slightly shifted from the radio peaks inward about 4′ (10 pc).

3. KINEMATICS OF THE HIGH-VELOCITY MOLECULAR STRUCTURES

The kinematical relation between the molecular and continuum features can be studied using (l, V) (position-velocity) diagrams at corresponding latitudes. The upper panel of Figure 1 shows an (l, V) diagram at $b = 8'$ of the ^{13}CO line. The eastern and western molecular spurs are recognized as the high-density clumps at (l, V) $\sim$ (8′, 100 km s^{-1}) and at ($-30'$, -150 km s^{-1}), respectively. The two clumps appear about symmetrical with respect to the center of the GCL, while slightly shifted toward negative velocity by about -20 km s^{-1}. In the same figure, we compare this (l, V) plot with the radio continuum map, where the GCL positions are marked by the thick lines, and the positional relation between radio and ^{13}CO features are indicated by the vertical lines. The symmetric appearance of the molecular clumps in the (l, V) plot with respect to the GCL center ($l \sim -10'$) suggests a physical connection of the molecular gas with the radio structure. The

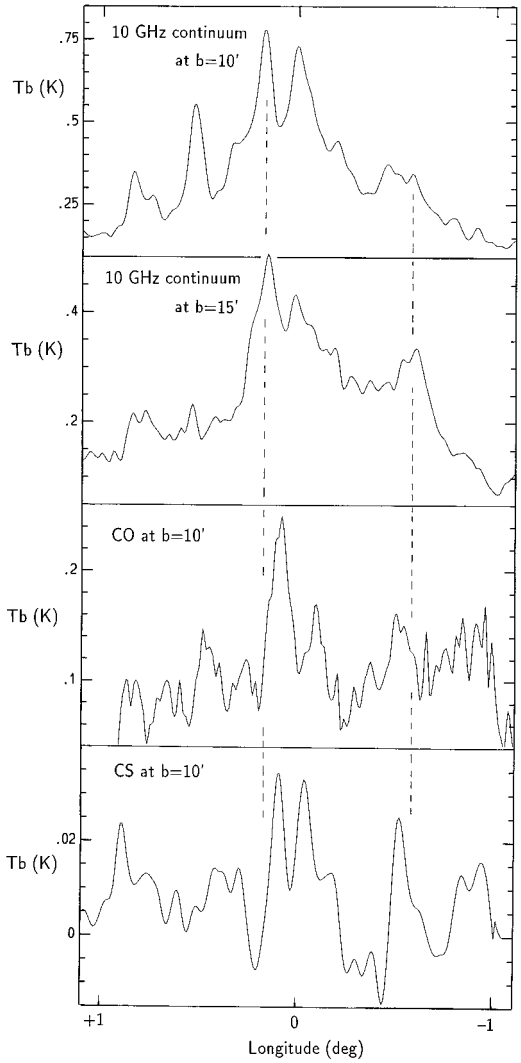

FIG. 3.—Cross sections of the radio continuum at $b = 10'$ and $15'$, CO and CS line intensities at $b = 10'$. Note that the intensity scale of the 10 GHz emission at $b = 10'$ is 1.6 times that at $15'$.

fact that the eastern clump is receding from us and the western clump approaching us may indicate a rotation of the GCL gas at ~100–150 km s^{-1}. The molecular spurs may be tangential views of a rotating torus or cylinder of gas in the lower part of the GCL.

Vertical kinematics along the GCL ridges can be obtained by (b, V) diagrams at corresponding longitudes. Figure 4 shows a composite (b, V) plot of the ^{13}CO line, where the positive-velocity half represents a (b, V) plot at $l = 10'$ for the eastern ridge and the negative-velocity half is at $l = -30'$ for the western ridge. The major emission at $-10' < b < 5'$ in the figure is due to a rotating molecular ring of larger radius (Sofue 1995a). The GCL molecular spurs are recognized as two tilted ridges at $b \sim +5'$–$15'$ with $V_{\rm LSR} \sim +100$ km s^{-1} and ~ -150 km s^{-1}, which appear symmetric with respect to $V_{\rm LSR} = 0$ km s^{-1}. The tilt in the (b, V) plot indicates a velocity gradient along the spur ridge in the sense that $|V_{\rm LSR}|$ increases with the height from the disk plane.

4. DISCUSSION

The mass of the high-velocity molecular clumps (spurs) can be estimated from the CO line intensity. We assume a conversion factor from the ^{12}CO ($J = 1$–0) intensity to H_2 column density of $\sim 0.92\ (\pm 0.2) \times 10^{20}$ H_2 cm^{-2} K^{-1} km s^{-1} derived for the Galactic center (Arimoto, Sofue, & Tsujimoto 1996) and take the ^{12}CO/^{13}CO intensity ratio of about 6.2 (Solomon, Scoville, & Sanders 1979). From Figure 3, the averaged excess of the ^{13}CO intensity within the $10' \times 10'$ (25 pc $\times$ 25 pc) region of each molecular clump is 0.06 (± 0.02) K $\times$ 500 km s^{-1} $\simeq$ 30 (± 10) K km s^{-1}. This yields an H_2 column density of $1.7\ (\pm 0.6) \times 10^{22}$ H_2 cm^{-2}. This corresponds to a density of ~100 H_2 cm^{-3}, if the spurs are tangential views of a cylinder with a line-of-sight depth of ~50 pc. For the Galactic center distance of 8.5 kpc, we obtain a total H_2 mass of $\sim 3.3\ (\pm 1) \times 10^5\ M_\odot$ within the two GCL molecular clumps. If the observed clumps are tangential parts of a cylinder, the total mass would be larger. In fact, we can recognize some excess gas at $V_{\rm LSR} \sim -50$ km s^{-1} in Figure 1, which may be part of the cylinder. The kinetic energy of the gas clumps at velocities ± 150 km s^{-1} is of the order of 7×10^{52} ergs. This amount is not surprising if it is due to the Galactic rotation balancing the gravitational potential of the stellar mass of $\sim 10^8\ M_\odot$.

Three possible models have been proposed for the origin of the GCL:

Cylindrical outflow model.—This model predicts that the disk gas is vertically accelerated along the poloidal magnetic field when the field lines are twisted by accretion of the rotating nuclear disk (Uchida, Shibata, & Sofue 1985). The cylinder structure in this model is consistent with the radio cross section of the GCL (Sofue 1985). The outflow velocity is estimated to be of the order of the Alfvén velocity and is ~150 km s^{-1} for a gas density of ~100 H_2 cm^{-3} and magnetic field of a milligauss. In addition, the whole cylinder with gas must be rotating at the disk rotation speed, which is consistent with the observed high-velocity rotation in the (l, V) plot comparable to the Galactic rotation (Fig. 1). The systematic velocity shift of -20 km s^{-1} in the (l, V) plot could be accounted for if the cylinder axis (outflow axis) is inclined by ~8° toward the Sun. The velocity gradient in the b-direction (Fig. 4, Pl. L12) could be accounted for if the magnetic cylinder is conical, so that the rotation velocity increases with the distance from the disk. The inward displacement of the molecular gas ridges from the radio ridges (Fig. 3) and the displacement of the cylinder axis from $l = 0'$ remain an open question. The gas versus magnetic field location would depend on the initial configuration of the poloidal field and accretion disk, and a detailed modeling is desired (Uchida et al. 1985).

Magnetic loop model.—The GCL may be an Ω-like inflating magnetic loop anchored to the magnetized nuclear disk (Sofue & Handa 1984). As the loop is rotating with the disk, the high-velocity rotation would also be naturally understood. However, the gas in such a loop may be falling down toward the disk along the magnetic tube, and, therefore, the vertical velocity gradient would reflect a deceleration of the falling motion near the roots.

Explosion model.—Finally, the GCL may be an expanding shock front associated with an explosion near the nucleus (Sofue 1984). The GCL would then be a dumbbell-shaped gaseous shell accumulated from the inner region, and, therefore, the rotation must be small due to the angular-momentum

conservation. The observed high velocities would then be due to a line-of-sight effect of localized expanding gas clumps at large azimuthal angles from the node. The vertical velocity gradient would be due to a faster expansion into the halo than into the disk.

According to the discussion above, we may conclude here that the cylindrical outflow model appears the most plausible among the three models.

The author thanks J. Bally for making the BTL survey database available.

REFERENCES

Arimoto, N., Sofue, Y., & Tsujimoto, T. 1996, PASJ, in press
Bally, J., Stark, A. A., Wilson, R. W., & Henkel, C. 1987, ApJS, 65, 13
Sofue, Y. 1984, PASJ, 36, 539
———. 1985 PASJ, 37, 697
———. 1995a PASJ, 47, 527
———. 1995b PASJ, 47, 551
Sofue, Y., & Handa, T. 1984, Nature, 310, 568
Sofue, Y., Reich, W., Inoue, M., & Seiradakis, J. H. 1987, PASJ 39, 95
Solomon, P. M., Scoville, N. Z., & Sanders, D. B. 1979, ApJ, 232, L89
Tsuboi, M., Inoue, M., Handa, T., Tabara, H., Kato, T., Sofue, Y., & Kaifu, N. 1986, AJ, 92, 818
Uchida, Y., Shibata, K., & Sofue, Y. 1985, Nature 317, 699
Yusef-Zadeh, F., Morris, M., & Chance, D. 1984, Nature, 310, 557

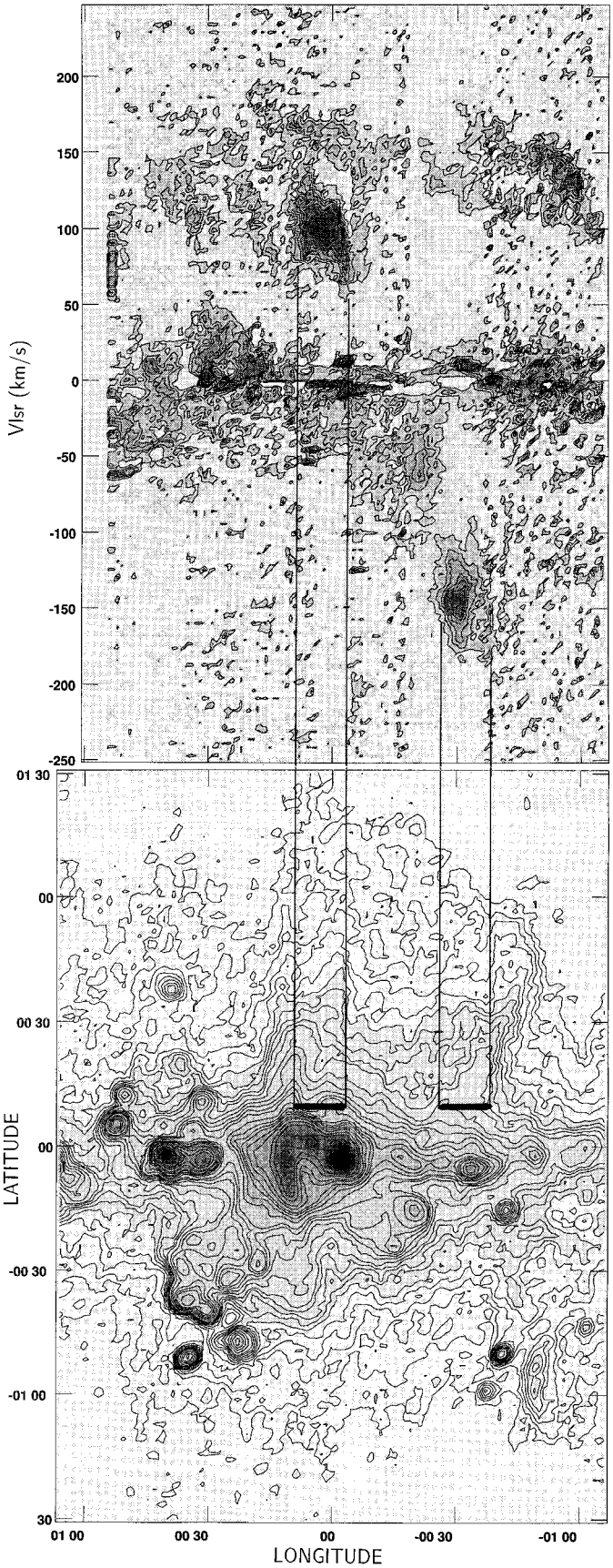

FIG. 1.—10.5 GHz radio continuum map of the Galactic center (*lower panel*) and a ^{13}CO (l, V) diagram at $b = 8'$ (*top panel*). High-velocity CO clumps are associated with the ridges of the Galactic center radio lobe. CO and radio contours are at 1, 2, . . . , 10, 12, . . . , 20, 25, . . . , 40 × 0.2 and 0.03 K, respectively.

PLATE L11

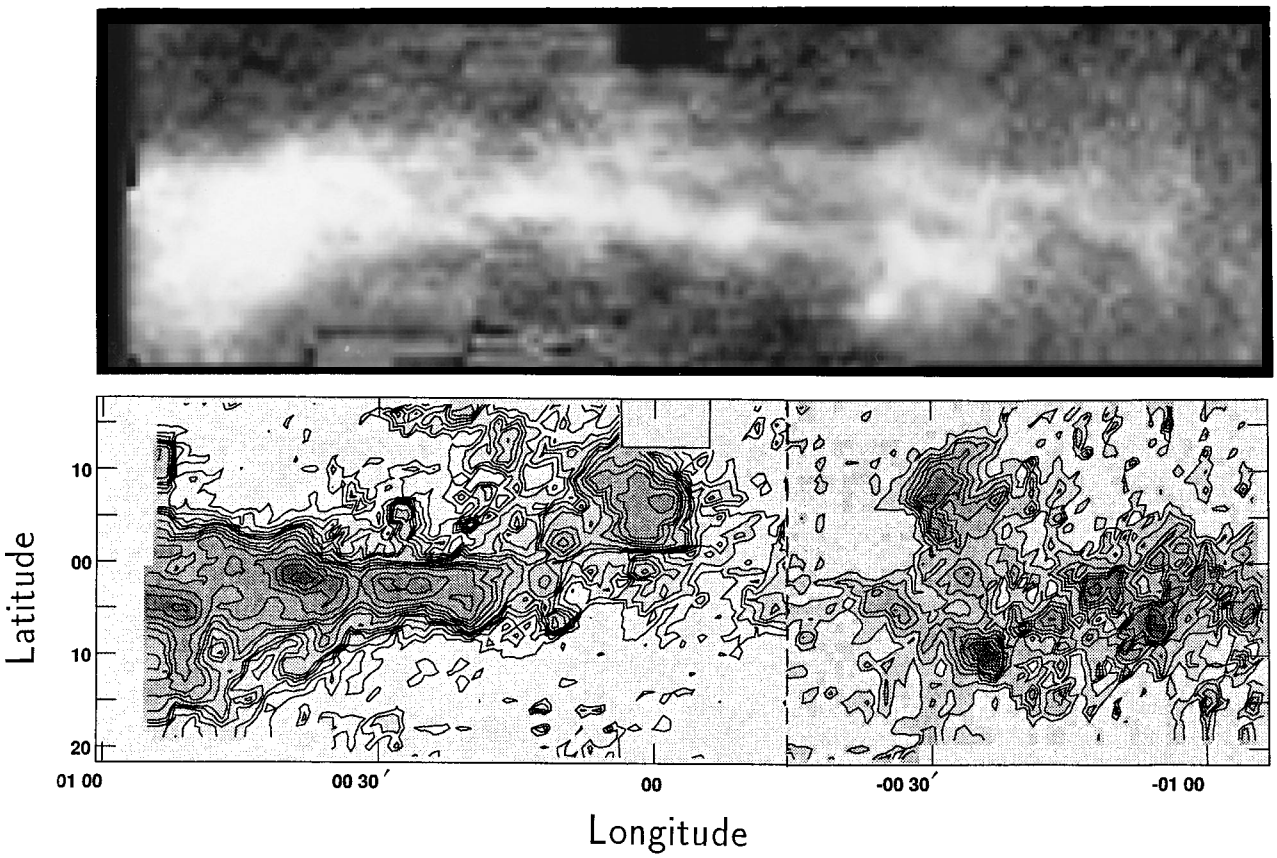

FIG. 2.—*Top panel*: ^{13}CO total intensity map (Bally et al. 1987). *Bottom*: Composite CO intensity map integrated from -160 to -150 km s^{-1} for the eastern half and from $+90$ to $+100$ km s^{-1} for the western half. Contours are at 1, 2, . . . , 10, 12, 15, 20, . . . , 40, 50, . . . , 80 $\times$ 0.1 K.

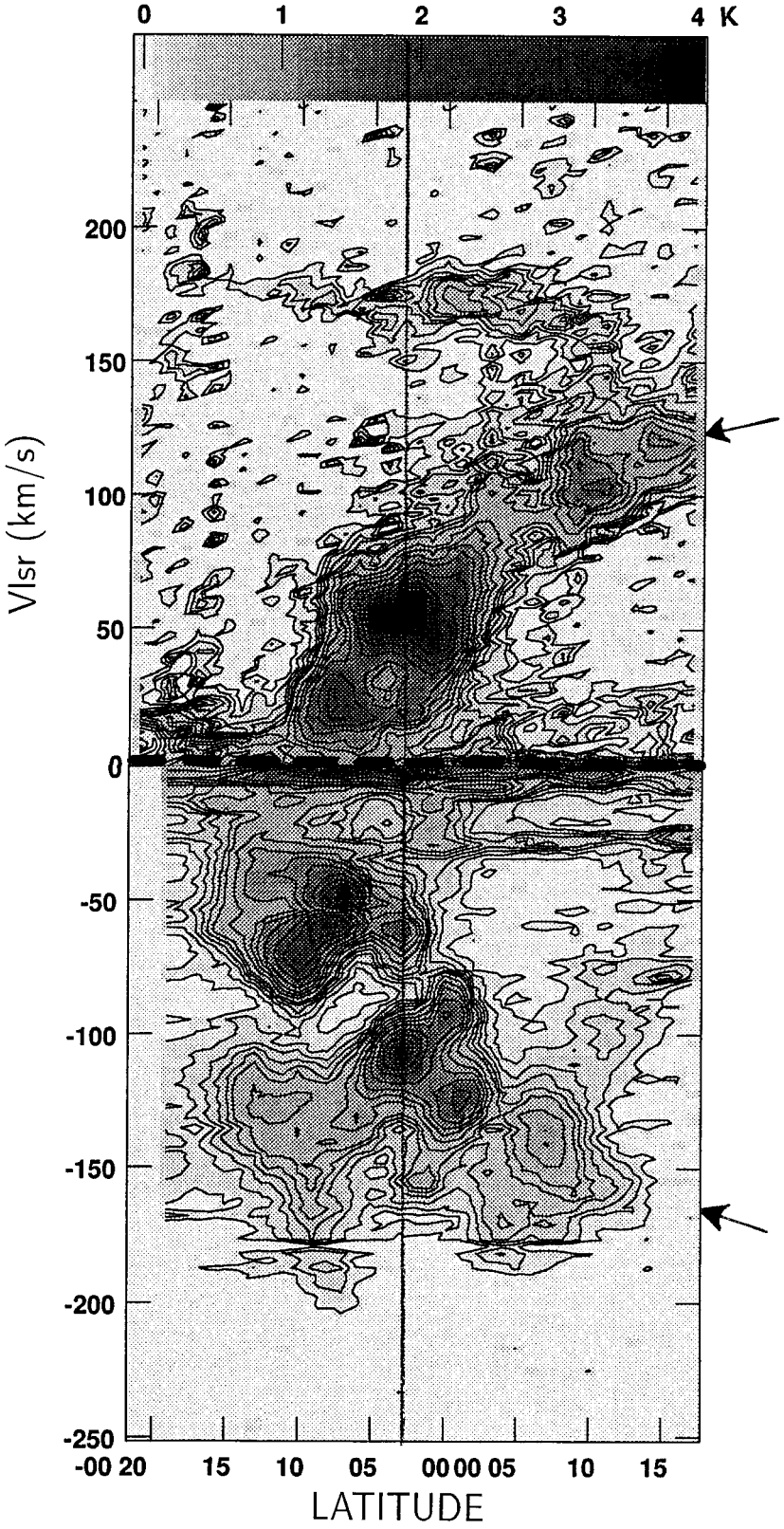

FIG. 4.—Composite (b, V) diagram of the CO emission. The upper half ($V_{LSR} > 0$) is along the eastern ridge at $l = 10'$, and the lower half ($V_{LSR} < 0$) along the western ridge at $l = -30'$. Contours are at 1, 2, . . . , 10, 12, 15, 20, . . . , 40 × 0.1 K.